Electrical and Optical Properties of Radio-Frequency-Sputtered Thin Films of $(ZnO)_5In_2O_3$

Hidenori Hiramatsu, Won-Seon Seo, and Kunihito Koumoto*

Department of Applied Chemistry, Graduate School of Engineering, Nagoya University, Furo-cho, Chikusa-ku, Nagoya 464-8603, Japan

Received March 23, 1998. Revised Manuscript Received June 29, 1998

c-Axis oriented thin films of $(ZnO)_5In_2O_3$ of 0.5 μm thickness were deposited on glass substrates by a radio-frequency-sputtering method. The thin films had dense columnar structures and were highly transparent in the ultraviolet−visible region, simultaneously showing low electrical resistivity. The refractive index was about 2. The lowest resistivity, 1.3×10^{-3} Ω cm at room temperature, was obtained by reducing the deposited film at 540 °C in N_2 containing 3.4% H_2. The corresponding carrier concentration and Hall mobility were 1.9×10^{20} cm^{-3} and 25.6 cm^2/Vs, respectively. Detailed analyses of the optical transmittance spectra gave rise to the intrinsic band gap and the reduced mass of carriers to be 3.12 eV and 0.67 m_0, respectively.

Introduction

Thin films with low electrical resistivity and optical transparency in the ultraviolet−visible region have been applied to transparent electrodes for photoelectric energy conversion devices, such as solar cells and liquid crystal display (LCD). The transparent conductive thin films are usually made of degenerate n-type semiconducting oxides with wide band gaps of 3−4 eV. Some representative oxide materials include tin-doped indium oxide (ITO),[1,2] fluoride-doped tin oxide (SnO_2)[3] and aluminum-doped zinc oxide (ZnO).[4,5] Transparent conductive materials with higher conductivity are, however, required to develop high-quality LCDs, and various materials containing ZnO, such as $InGaZnO_4$,[6] $Zn_2In_2O_5$,[7] and $ZnSnO_3$,[8] and those containing In_2O_3, such as $MgIn_2O_4$,[9,10] $InGaMgO_4$,[11] and $GaInO_3$,[12] have been investigated. Recently transparent p-type semiconducting $CuAlO_2$ has been reported to show high performance, and a functional window composed of a transparent p−n junction is proposed.[13]

We have reported that the homologous compounds in the $ZnO-In_2O_3$ system, $(ZnO)_kIn_2O_3$ (k = an integer ≥3), show fairly high electrical conductivity and high electron mobility.[14,15] These homologous compounds have very unique crystal structures belonging to the space groups $R\bar{3}m$ (for k = odd) or $P6_3/mmc$ (for k = even) and are composed of the layers of $InO_{2/3}$, $(InZnO)_{5/2}$, and ZnO, which are stacked sequentially along the *c*-axis of the hexagonal system.[16−18] We also reported that *c*-axis- and (110)-plane-oriented $(ZnO)_5In_2O_3$ films prepared by a radio-frquency(rf)-sputtering technique using a complex target consisting of 50 small pellets of $(ZnO)_5In_2O_3$ placed on a large plate of ZnO had shown different thermoelectric properties, and it was clarified that the electron mobility along the *c*-plane is much larger than along the *ab*-plane.[19]

In the present study, we prepared *c*-axis-oriented $(ZnO)_5In_2O_3$ thin films by a rf-sputtering method using a sintered target of single-phase $(ZnO)_5In_2O_3$ in order to accelerate the deposition rate and achieve stable sputtering conditions, to obtain high crystallinity and homogeneity. In this paper the electrical and optical properties of the *c*-axis-oriented $(ZnO)_5In_2O_3$ thin films are reported.

* Corresponding author. TEL: +81-52-789-3327. FAX: +81-52-789-3201. E-mail: g44233a@nucc.cc.nagoya-u.ac.jp.

(1) Nagatomo, T.; Maruta, Y.; Omoto, O. *Thin Solid Films* **1990**, *192*, 17.
(2) Ray, S.; Banerjee, R.; Basu, A.; Batabyal, A. K.; Barua, A. K. *J. Appl. Phys.* **1983**, *54*, 3497.
(3) Banerjee, R.; Das, D. *Thin Solid Films* **1987**, *149*, 291.
(4) Minami, T.; Nanto, H.; Takata, S. *Jpn. J. Appl. Phys.* **1984**, *23*, L280.
(5) Minami, T.; Nanto, H.; Takata, S. *Jpn. J. Appl. Phys.* **1985**, *24*, L605.
(6) Orita, M.; Sakai, H.; Takeuchi, M.; Yamaguchi, Y.; Fujino, T.; Kojima, I. *Trans. Mater. Res. Soc. Jpn.* **1996**, *20*, 573.
(7) Minami, T.; Sonohara, H.; Kakumu, T.; Tanaka, S. *Jpn. J. Appl. Phys.* **1995**, *34*, L971.
(8) Minami, T.; Sonohara, H.; Takata, S.; Sato, H. *Jpn. J. Appl. Phys.* **1994**, *33*, L1693.
(9) Kawazoe, H.; Ueda, N.; Un'no, H.; Omata, T.; Hosono, H.; Tanoue, T. *J. Appl. Phys.* **1994**, *76*, 7935.
(10) Hosono, H.; Un'no, H.; Ueda, N.; Kawazoe, H.; Matsunami, N.; Tanoue, H. *Nucl. Inst. Methods Phys. Res.* **1995**, *B106*, 517.
(11) Orita, M.; Takeuchi, M.; Sakai, H.; Tanji, H. *Jpn. J. Appl. Phys.* **1995**, *34*, L1550.
(12) Phillips, J. M.; Kwo, J.; Thomas, G. A.; Carter, S. A.; Cava, R. J.; Hou, S. Y.; Krajewski, J. J.; Marshall, J. H.; Peck, W. F.; Rapkine, D. H.; van Dover: R. B. *Appl. Phys. Lett.* **1994**, *65*, 115.
(13) Kawazoe, H.; Yasukawa, M.; Hyodo, H.; Kurita, M.; Yanagi, H.; Hosono, H. *Nature* **1997**, *389*, 939.
(14) Ohta, H.; Seo, W. S.; Koumoto, K. *J. Am. Ceram. Soc.* **1996**, *79*, 2193.
(15) Kazeoka, M.; Hiramatsu, H.; Seo, W. S.; Koumoto, K. *J. Mater. Res.* **1998**, *13*, 523.
(16) Kasper, H. *Z. Anorg. Allg. Chem.* **1967**, *349*, 113.
(17) Cannard, P. J.; Tilley, R. J. D. *J. Solid State Chem.* **1988**, *73*, 73.
(18) Nakamura, M.; Kimizuka, N.; Mohri, T. *J. Solid State Chem.* **1990**, *86*, 16.
(19) Hiramatsu, H.; Ohta, H.; Seo, W. S.; Koumoto, K. *J. Jpn. Soc. Powder Powder Metall.* **1997**, *44*, 44.

10.1021/cm980173b CCC: $15.00 © 1998 American Chemical Society
Published on Web 09/12/1998

Experimental Section

Target Preparation. The starting powders of ZnO and In_2O_3 (purity 99.99%, average particle size of 1 μm for both powders; Kojundo Chemical Laboratory Co.) were mixed in ethanol and ball-milled for 48 h. The resulting powder was then filtered and dried. The dried powder was mixed with binders (10 wt % liquid paraffin and 5 wt % *n*-heptane), uniaxially pressed into a disk 95 mm in diameter, and further pressed isostatically under the pressure of 98 MPa to eliminate laminations and cracks in the disk. The disk was calcined at 1000 °C for 1 h, to remove binders in a vented electric furnace, and then cooled to room temperature. The disk was further reaction-sintered at 1550 °C for 2 h in air and then rapidly cooled to room temperature. After its surface was polished, the reaction-sintered single-phase $(ZnO)_5In_2O_3$ disk was employed for the sputtering target. Our preliminary experiment included an attempt to fabricate single-phase targets of other compositions, i.e., $k = 3$ and 7. However, the starting composition of $k = 3$ always gave rise to $k = 4$ and unreacted In_2O_3, and a single-phase target could not be obtained by the reaction-sintering method. The target with $k = 7$ was successfully obtained, but the sputtered films synthesized under various conditions only showed poor crystallographic orientations and hence poor electrical properties. Consequently, we decided that this paper should concentrate on the $k = 5$ composition for simplicity and clarity.

Thin-Film Deposition. Thin films of $(ZnO)_5In_2O_3$ were prepared on Corning #7059 glass substrates in a rf-sputtering apparatus (ULVAC, SBR-1104). The sputtering chamber was evacuated by a rotary and diffusion pumping unit (limit pressure 2×10^{-6} Torr (2.66×10^{-4} Pa)). The target-to-substrate distance was fixed to be 30 mm, and the temperature of the substrate was maintained at 300 °C during sputtering. After the target was presputtered for about 15 min, the deposition of a film was carried out at the rf power of 25−75 W (13.56 MHz) for 1 h under the chamber pressure of 7.5−50 mTorr (1.0−6.7 Pa). Ar or Ar/O_2 mixed gas (4.8% O_2) was used as the sputtering gas to find the optimum deposition conditions to obtain *c*-axis-oriented films of $(ZnO)_5In_2O_3$ stoichiometry. After optimizing the deposition conditions, the deposition time was varied from 30 to 90 min, and then the thickness of a film was determined by using a surface roughness detector with a stylus (Kosaka Laboratory Co., ET-30) in order to calculate the deposition rate. Final thicknesses of the thin films for physical measurement and characterization were controlled to be ∼0.5 μm.

Thin-Film Annealing and Reduction. The electrical resistance of as-deposited $(ZnO)_5In_2O_3$ films was very large in all cases. To attain higher conductivity, the films were annealed under Ar or N_2/H_2 (the H_2 concentration was varied from 0.5 to 4.0%) at 500−600 °C for 1−3 h to relax internal stress, to increase the crystallinity, and to partially reduce them.

Characterization. X-ray diffraction (XRD, $2\theta/\theta$ continuous scan, 2θ 10°−60°) and pole figure measurements (Shultz reflection, $\alpha' = 20°- 90°$, $\beta = 0°- 360°$) using Cu Kα radiation were carried out to identify the crystalline phases and crystallographic orientation (RIGAKU, RINT-2100), respectively. Metal compositions of the thin films, i.e., Zn/In ratios, were analyzed by X-ray fluorescence spectrometry (XRF, HORIBA, EMAX-5770) after gold was dc-sputtered ∼5 nm thick on their surfaces. Microstructures of the surface and the cross section were observed with a field emission scanning electron microscope (FE-SEM, HITACHI, S-4100). Thin films were very flat, so all images were taken by tilting them at 45° to obtain enough contrast.

Properties. The resistivity (ρ), carrier concentration (n), and Hall mobility (μ) of the thin films were estimated from Hall effect measurements, conducted at room temperature with a GP−IB operating system (TOYO TEKUNIKA Co. RESITEST 8200). A homemade apparatus with four Au probes (S. E. R. Co., MS0011-10) was employed for Hall measurements by the van der Pauw method[20] to obtain ohmic contact and small contact resistance. The applied current and magnetic field were 1 mA and 5 kG, respectively, for all the Hall measurements. The optical transmission spectra of the thin films were measured at room temperature in the wavelength range from 300 to 2600 nm (Hitachi, U-3410) using Corning #7059 glass substrate as a reference.

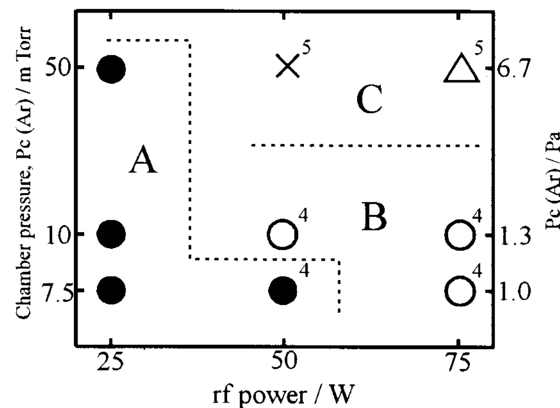

Figure 1. The dependence of the crystal-axis orientation, the crystallinity, and the composition of the thin films on the rf power and the chamber pressure: ○, *c*-axis oriented film; ×, nonoriented film; △, (110)-plane oriented film; ●, poor crystallinity. Superscripts, 4 and 5, indicate the composition of the thin films, k in $(ZnO)_kIn_2O_3$.

Results and Discussion

Optimization of the Deposition Conditions. The first experiments were carried out with Ar for the sputtering gas, changing mainly the rf power and the chamber pressure, while the deposition time was fixed at 1 h, to search for the optimum sputtering conditions to obtain *c*-axis-oriented thin films of $(ZnO)_5In_2O_3$. Figure 1 shows the orientation, the crystallinity, and the composition of the as-deposited thin film depending on rf power and chamber pressure. The manner of orientation and composition can be divided into three categories (A, B, and C) in the rf power − chamber pressure diagram as shown in Figure 1. The A group thin films revealed *c*-axis orientation with the *c*-planes aligned parallel to the film surfaces, but they were inferior to the others in crystallinity, and their compositions were poor in Zn, i.e., $k = 4$. The B group thin films also revealed *c*-axis orientation and they were superior to the others in crystallinity, but they were also poor in Zn. The C group thin films did not show *c*-axis orientation, but the compositions of the films were nearly the same with that of the target, i.e., $k = 5$.

Second experiments were carried out with Ar/O_2 (4.8% O_2) as the sputtering gas, changing mainly the chamber pressure, while the deposition time was again fixed to be 1 h. Figure 2 shows the XRD patterns of $(ZnO)_kIn_2O_3$ thin films deposited at the rf power of 50 W. Under the chamber pressure of 10−30 mTorr (1.3−4.0 Pa), the compositions appeared to be poor in Zn. In contrast, under the chamber pressure of 35−50 mTorr (4.7−6.7 Pa) the composition became similar to that of the target, and those deposited under a chamber pressure of 35 mTorr (4.7 Pa) revealed the highest crystallinity and *c*-axis orientation (perpendicular to substrate). How-

(20) van der Pauw, L. J. *Philips Res. Rep.* **1958**, *13*, 1.

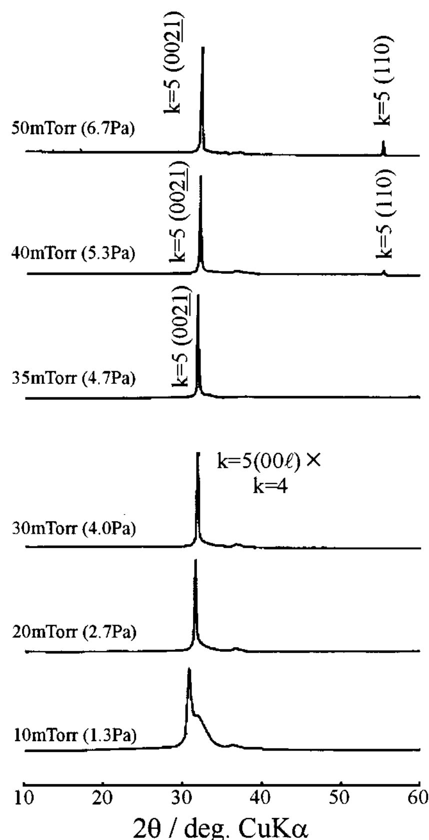

Figure 2. XRD patterns of the thin films of $(ZnO)_kIn_2O_3$ deposited at the rf power of 50 W for 1h under Ar/O_2 mixture gas.

Table 1. Optimized Deposition Conditions for *c*-Axis-Oriented Thin Films of $(ZnO)_5In_2O_3$

rf power	50 W
substrate temperature	300 °C
sputtering gas composition	95.2% Ar, 4.8% O_2
chamber pressure	35 mTorr (4.7 Pa)
deposition rate	12 nm/min

ever, XRD patterns of $(ZnO)_kIn_2O_3$ thin films deposited at the rf power of 75 W all showed no specific orientation, though the reason is not well-known; one possible reason is that the rf power was so high that the back-sputtered particles might have inhibited the oriented growth of a film.

The final optimized sputtering conditions for the deposition of the *c*-axis-oriented thin films of stoichiometry $(ZnO)_5In_2O_3$ with 0.5 μm thickness are shown in Table 1.

Optimized Thin Film. The XRD pattern of the film deposited under the optimized conditions exhibited sharp reflection from $(00\underline{21})$ planes as shown in Figure 3. The peak position of $(00\underline{21})$ of the as-deposited film was shifted to the lower angle side compared to that of a bulk polycrystal.[21] However, the peak was shifted back to the standard bulk position after the film was annealed under Ar or N_2 containing H_2, as shown in Figure 3. This result indicates that the shift was caused by internal stress, possibly induced by thermal expansion mismatch between the film and the substrate. The X-ray pole figure of the thin film from $(00\underline{21})$ for $\{01\underline{11}\}$ planes was a concentric circle at about $\alpha' = 32°$, as shown in the inset of Figure 3, indicating that the optimized film consists of polycrystals with their *c*-axes oriented perpendicular to the substrate and their *a*-axes randomly oriented.

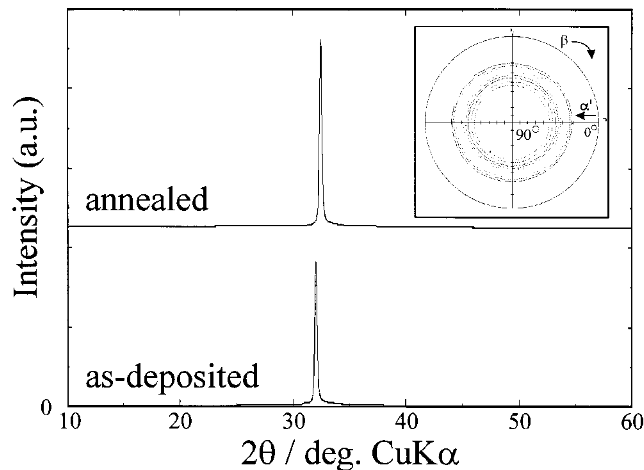

Figure 3. XRD patterns of *c*-axis-oriented thin films of $(ZnO)_5In_2O_3$ deposited under the optimized conditions. The inset shows the X-ray pole figure of the annealed film from $(00\underline{21})$ for $\{01\underline{11}\}$ planes.

Microstructure. Figure 4 shows typical FE-SEM images of the surface and the cross section of an as-deposited thin film. It is seen that the thin film has dense columnar structure with the column diameter ranging from 20 to 70 nm. These columns are densely packed to form a film (Figure 4a), while the average length of the single column appears to be smaller than the film thickness, indicating that the film is composed of a few columnar particles in the thickness direction (Figure 4b).

Crystallographically oriented columnar structures can often be observed in sputtered thin films.[19,22,23] According to the model suggested by Thornton,[23] dense columnar structures are formed in a film when the substrate temperature is lower than about a half of the melting point of the film. The substrate temperature employed in the present study (300 °C) was far lower than a half of the melting point of $(ZnO)_5In_2O_3$ (>1600 °C).

The surface of a thin film annealed under Ar was flatter than that of the as-deposited thin film, though the columnar structure remained unchanged and the grain growth did not apparently take place. Figure 5 shows typical FE-SEM images of the surface of a thin film reduced by N_2 containing H_2. It is obvious that the pores with diameter from 30 to 80 nm were produced only in the surface region of the thin film by the reduction treatment. An as-deposited film must have contained some regions with inhomogeneous compositions which can be easily decomposed by reduction. This may be the reason annealing in a reducing atmosphere resulted in pore formation.

Electrical Properties. *Ar-Annealed Thin Films.* Figure 6 shows the electrical resistivity (ρ), carrier concentration (n), and Hall mobility (μ) of *c*-axis-oriented $(ZnO)_5In_2O_3$ thin films annealed under Ar. The Hall coefficients were always negative, indicating that all the specimens were n-type semiconductors. It can be seen

(21) JCPDS card No. 20-1440, 1967.

(22) Patten, J. W.; McClanahan, E. D. *J. Appl. Phys.* **1972**, *43*, 4811.
(23) Thornton, J. A. *J. Vac. Sci. Technol.* **1974**, *11*, 666.

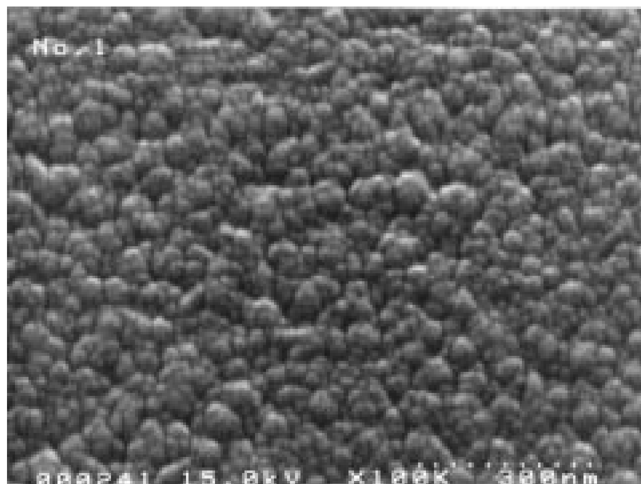

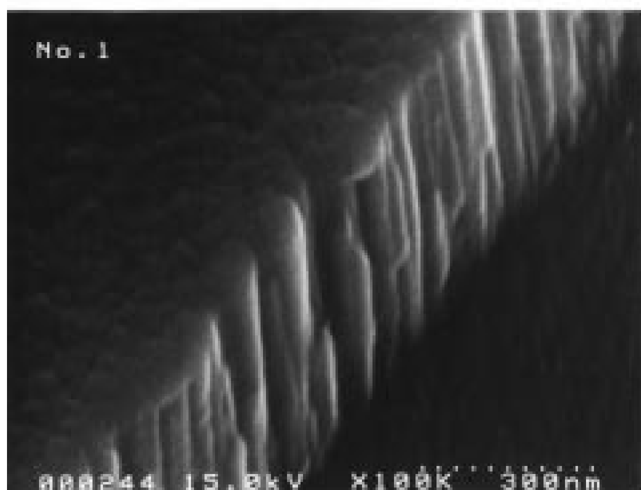

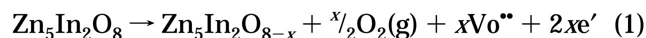

Figure 4. Typical FE-SEM photographs of (a) the surface and (b) the cross section of the as-deposited thin film (tilted at 45°).

in the figure that carrier concentration, n, increased with increasing annealing temperature and resistivity, ρ, decreased with increasing n, while the mobility, μ, showed the maximum at the annealing temperature of ~550 °C.

Carrier electrons must have been generated by the following reaction taking place during annealing under Ar,

$$Zn_5In_2O_8 \rightarrow Zn_5In_2O_{8-x} + {}^{x}/_{2}O_2(g) + xVo^{\bullet\bullet} + 2xe' \quad (1)$$

where $Vo^{\bullet\bullet}$ denotes an oxide ion vacancy and e′ denotes an electron. This reaction indicates basically the reduction of a film, and it can be explained by taking into account the lower oxygen partial pressure of Ar [estimated to be 10^{-4} atm (10 Pa)] than the sputtering gas (Ar/O_2 mixture).

The result that the Hall mobility of carrier electrons showed the maximum at certain annealing temperature is rather interesting, and it can be explained by assuming that the mobility is associated with the internal stress. It is known that the internal stress (σ_{stress}) and

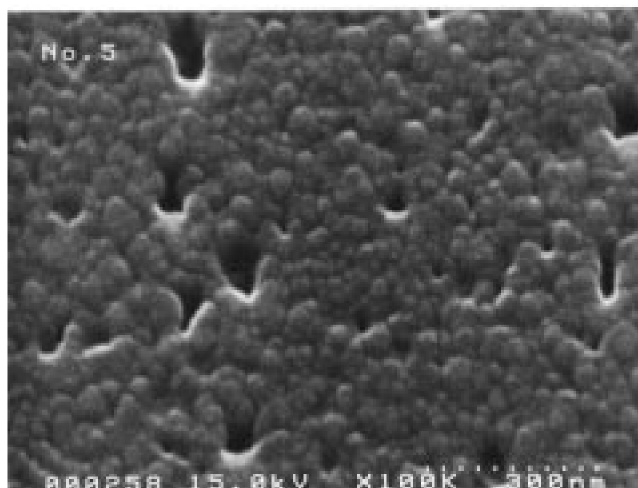

Figure 5. Typical FE-SEM photograph of the surface of the thin film reduced by H_2 (tilted at 45°).

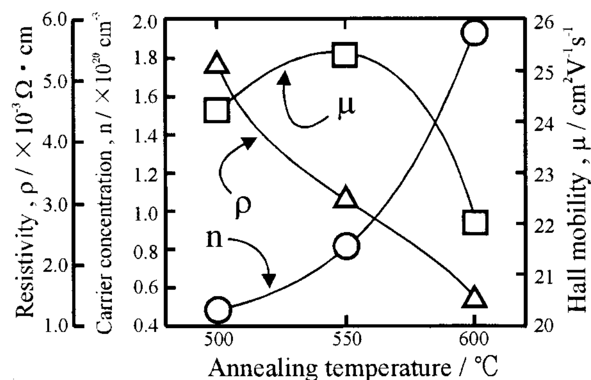

Figure 6. Resistivity (ρ), carrier concentration (n), and Hall mobility (μ) of c-axis-oriented thin films of $(ZnO)_5In_2O_3$ as functions of annealing temperature under Ar.

strain (ϵ) for the thin film are respectively given by the following equations,[24]

$$\sigma_{stress} = \frac{E\epsilon}{2\nu} \quad (2)$$

$$\epsilon = (d_{0hkl} - d_{hkl})/d_{hkl} \quad (3)$$

where E, ν, d_{0hkl}, and d_{hkl} are Young's modulus of the substrate, Poisson's ratio of the substrate, the stress-free interplanar distance of (hkl) planes, and the measured interplanar distance, respectively. Figure 7 shows the internal stress of the c-axis-oriented $(ZnO)_5$-In_2O_3 films as a function of annealing temperature calculated using eqs 1 and 2, and the temperature dependence of Hall mobility μ is shown for comparison. The σ_{stress} decreased with increasing annealing temperature and showed the minimum value of 135 MPa at ~500 °C. The annealing temperature dependence of σ_{stress} is opposite to that of μ, though not completely, strongly suggesting that the internal stress suppresses the electronic conduction in the film and its removal by annealing at an appropriate temperature enhances the mobility of electrons.

(24) Light, T. B.; Wagner, C. N. J. *J. Vac. Sci. Technol.* **1966**, *3*, 1.

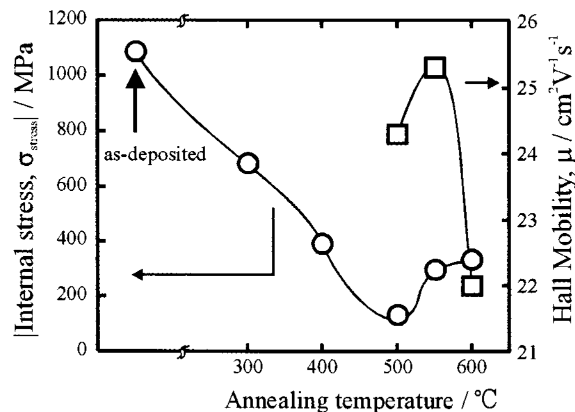

Figure 7. Relationship among the internal stress (σ_{stress}), Hall mobility (μ), and annealing temperature.

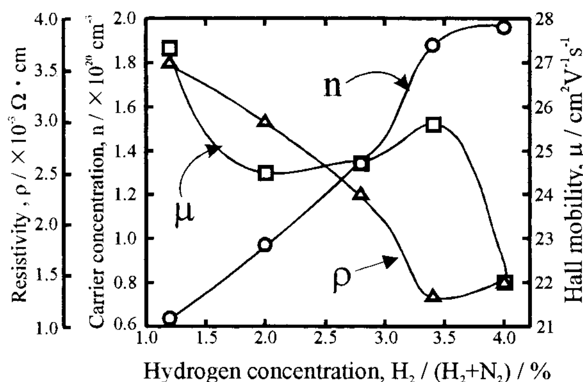

Figure 8. Resistivity (ρ), carrier concentration (n), and Hall mobility (μ) of *c*-axis-oriented thin films of $(ZnO)_5In_2O_3$ annealed at 540 °C for 1 h under N_2 containing various amounts of H_2.

The lowest ρ value of the thin film annealed under Ar was 1.5×10^{-3} Ω cm, and the corresponding n and μ were about 1.9×10^{20} cm^{-3} and 22.0 cm^2/V s, respectively.

The distorting and softening points of Corning #7059 glass substrate are respectively 593 and 844 °C, indicating that 600 °C is about the highest annealing temperature to yield films with low internal stress and yet inhibit alkaline metals in the substrate from diffusing into the films.

H_2-Annealed Thin Films. The *c*-axis-oriented $(ZnO)_5$-In_2O_3 thin films were annealed in N_2 containing 1.2–4.0% H_2 at various temperatures for 1 h. A preliminary experiment revealed that the thin films annealed above 550 °C were lacking Zn and became less transparent, so that the optimum reduction temperature was determined to be 540 °C. Figure 8 shows ρ, n, and μ as a function of the hydrogen concentration, $1.0 < H_2/(N_2 + H_2) \leq 4.0$. The lowest ρ value, 1.3×10^{-3} Ω cm, was obtained when the film was annealed under $H_2/(N_2 + H_2) = 3.4\%$. This condition gave rise to n and μ values of about 1.9×10^{20} cm^{-3} and 25.6 cm^2/V s, respectively, similar to those obtained for Ar-annealed films. In this case, carrier electrons must have been generated by partial reduction according to the following reaction:

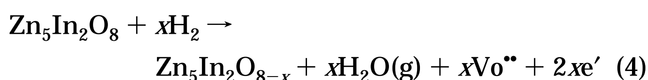

$$Zn_5In_2O_8 + xH_2 \rightarrow Zn_5In_2O_{8-x} + xH_2O(g) + xV_O^{\bullet\bullet} + 2xe' \quad (4)$$

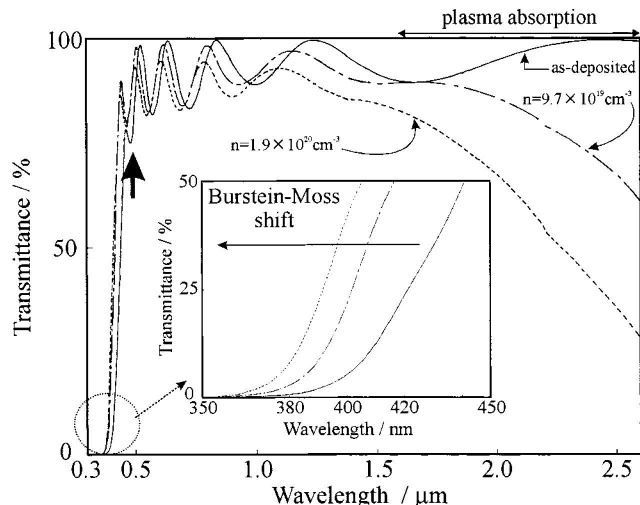

Figure 9. Typical transmittance spectra for *c*-axis-oriented thin films of $(ZnO)_5In_2O_3$ with various carrier concentrations. The inset shows the shift in the absorption edge.

Comparison of Figures 6 and 8 clearly indicates that Ar annealing at 600 °C and H_2 annealing at 540 °C have a similar effect on generating carrier electrons. Although the pores were formed in the thin film by H_2 annealing, as shown in Figure 5, the Hall mobility obtained was larger than that of the film annealed at 600 °C under Ar. This fact would be due to the relaxation of internal stress in the thin film annealed at 540 °C under H_2. Even though the pores were formed, their effect on the Hall mobility was negligible, possibly because they existed only in the surface of the film; the average ratio of pore depth to film thickness can be estimated to be less than $^1/_{10}$.

Optical Properties. Figure 9 shows the typical transmittance spectra for *c*-axis-oriented $(ZnO)_5In_2O_3$ thin films with various carrier concentrations. The inset shows the magnified portions of these spectra. The average transmittance of the as-deposited thin film was over 90% in the visible region, but it decreased to 85% with increasing carrier concentration. Slight absorption of the as-deposited thin film at about 450–500 nm, shown by an arrow in the figure, is due to the yellow color of the specimen. This absorption disappeared after annealing the film under Ar or $N_2 + H_2$, though the reason for this is not clear at present.

The refractive index (n_f) of the thin film in the wavelength region with only weak optical absorption is given by the following equations,[25]

$$n_f = [N + (N^2 - n_s 2)^{1/2}]^{1/2} \quad (5)$$

$$N = \frac{2n_s(T_{max} - T_{min})}{T_{max} \times T_{min}} + \frac{n_s^2 + 1}{2} \quad (6)$$

where n_s is the refractive index of the substrate (1.530 for the Corning #7059 glass substrate) and T_{max} and T_{min} are the comprehensive lines drawn through the maximum transmittance and the minimum transmittance, respectively, which appeared owing to the optical interference. Figure 10 shows the wavelength dependence of the refractive index n_f for the *c*-axis-oriented $(ZnO)_5$-

(25) Swanepoel, R. *J. Phys. E: Sci. Instrum.* **1983**, *16*, 1214.

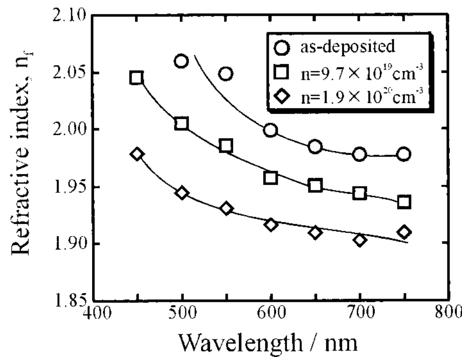

Figure 10. Wavelength dependence of the refractive index n_f for the *c*-axis-oriented thin films of $(ZnO)_5In_2O_3$ with various carrier concentrations.

In_2O_3 thin films. The n_f value slightly decreased with increasing carrier concentration, i.e., by annealing, which should be related to the relaxation of the internal stress of the thin film. The n_f values obtained at about 600 nm are 2.0 (as-deposited) and 1.9 ($n = 1.9 \times 10^{20}$ cm^{-3}), which were similar to that of ITO.[1,26]

An abrupt decrease in transmittance observed at the wavelength shorter than 500 nm is due to the fundamental absorption edge, which appears to be shifted toward the shorter wavelength side as the carrier concentrations increases. This shift, ΔE_{BM}, caused by the filling of the electronic states near the bottom of the conduction band, is well-known as the Burstein–Moss shift and is expressed by the following equation,[1,27]

$$\Delta E_{BM} = E_{gopt} - E_{g0} = \frac{h^2}{8m_{vc}}\left(\frac{3n}{\pi}\right)^{2/3} = \frac{\hbar^2}{2m_{vc}}(3n\pi^2)^{2/3} \quad (7)$$

where E_{gopt}, E_{g0}, h, and m_{vc} are the direct allowed optical band gap, the intrinsic band gap, Planck's constant, and the reduced mass ($m_{vc}^{-1} = m_e^{-1} + m_h^{-1}$, where m_e is the effective mass of an electron and m_h is the effective mass of a hole), respectively. At wavelength above 1.2 μm, the transmittance decreases abruptly because of the plasma absorption resulting from the high concentration of mobile electrons.[28] The increase in carrier concentration, owing to annealing and reduction, also shifts the plasma edge to shorter wavelength.

In the fundamental absorption region, the transmittance, T_{trans}, is given by the following equation,[29]

$$T_{trans} = A_1 \exp\left(\frac{-4\pi\kappa t}{\lambda}\right) \quad (8)$$

where κ, t, and A_1 are the extinction coefficient, the thickness of the thin film, and a constant, respectively. The preexponential term of eq 8 is negligibly small in this case, so that the absorption coefficient (α) can be defined as follows:

$$\alpha = \frac{4\pi\kappa}{\lambda} = \left(\ln\frac{1}{T_{trans}}\right)\frac{1}{t} \quad (9)$$

(26) Wu, W. F.; Chiou, B. S.; Hsieh, S. T. *Semicond. Sci. Technol.* **1994**, *9*, 1242.
(27) Burstein, E. *Phys. Rev.* **1954**, 93, 632.
(28) Chopra, K. L.; Major, S.; Pandya, D. K. *Thin Solid Films* **1983**, *102*, 1.
(29) Manifacier, J. C.; Fillard, J. P.; Bind J. M. *Thin Solid Films* **1981**, *77*, 67.

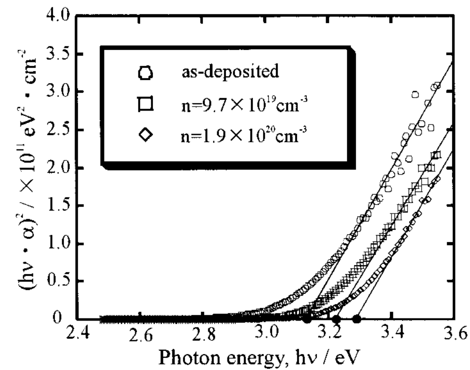

Figure 11. $(h\nu\alpha)^2$ vs $h\nu$ plots for the *c*-axi-oriented thin films of $(ZnO)_5In_2O_3$ with various carrier concentrations.

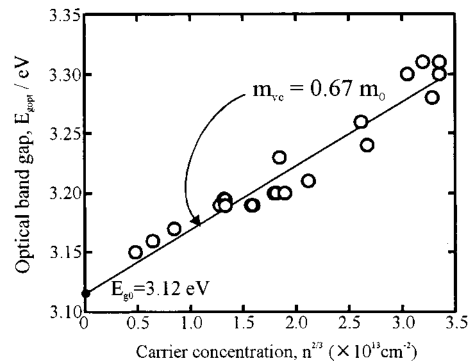

Figure 12. Dependence of the optical band gap on the carrier concentration.

On the other hand, when the optical transition probability is not zero, i.e., there exists an allowable transition, the optical energy dependence of the absorption coefficient for a direct allowed semiconductor is given by the following equation,[30]

$$\alpha = A_2\frac{(h\nu - E_{gopt})^{1/2}}{h\nu} \quad (10)$$

where E_{gopt} and A_2 are the optical band gap and a constant, respectively. Therefore, if the plots of $(h\nu\alpha)^2$ against $h\nu$ give rise to a straight line, the film can be regarded as a direct, allowed semiconductor and the optical band gap is given by extrapolating the straight line to the $h\nu$ axis. Figure 11 shows the representative plots of $(h\nu\alpha)^2$ against $h\nu$ for *c*-axis-oriented $(ZnO)_5In_2O_3$ thin films with various carrier concentrations. The straight line can be drawn through the data points in all cases, indicating firmly that $(ZnO)_5In_2O_3$ is a direct, allowed semiconductor.

The observed optical band gap increased from 3.15 to 3.31 eV with increasing carrier concentration. According to eq 7, the optical band gap depends linearly on $n^{2/3}$ and such dependence is clearly shown in Figure 12 when the experimental data for all the *c*-axis-oriented films prepared in the present study are plotted. The intrinsic band gap, E_{g0}, of $(ZnO)_5In_2O_3$ estimated from Figure 12 is 3.12 eV, and the reduced mass, m_{vc}, estimated from the slope of the straight line is $0.67m_0$, m_0 being the mass of a free electron.

The band gap of $(ZnO)_5In_2O_3$ is smaller than that of either ZnO (3.3 eV)[5] or In_2O_3 (3.75 eV),[30] and the

(30) Weiher, R. L.; Ley, R. P. *J. Appl. Phys.* **1966**, *37*, 299.

reduced mass is close to that of ITO (0.65 m_0).[2,31] These findings indicate that the Hall mobility of *c*-axis-oriented $(ZnO)_5In_2O_3$ thin films can be increased up to that of ITO, from 30 to 180 cm^2/Vs,[1,2] if carrier scattering could be suppressed, for instance by decreasing the number of grain boundaries, i.e., by grain growth.

Conclusions

c-Axis-oriented thin films of $(ZnO)_5In_2O_3$ with 0.5 μm thickness were deposited on Corning #7059 glass substrates by rf-sputtering. The optical transmittance of thin films was about 85% in the ultraviolet−visible region. The lowest resistivity obtained by annealing at 540 °C in N_2 containing 3.4% H_2 was as low as 1.3×10^{-3} Ω cm, and the corresponding carrier concentration and Hall mobility were 1.9×10^{20} cm^{-3} and 25.6 cm^2/V s, respectively. The results indicate that this material can be applied to transparent electrodes. The intrinsic band gap (3.12 eV) and the reduced mass (0.67m_0) were found to be comparable to those of ITO. Increase in the carrier mobility may be possible through better microstructure control.

Acknowledgment. The authors wish to thank H. Tanji, M. Orita, and K. Morita of HOYA Co. for the preparation of the sputtering target.

CM980173B

(31) Ohhata, Y.; Shinoki, F.; Yoshida, S. *Thin Solid Films* **1979**, *59*, 255.